

Project 2 - An Autoregressive Model for Bosonic Quantum Dots

Erlend Lima, Kristian Wold

I. INTRODUCTION

Problems in many-particle quantum mechanics is notoriously hard, and has over many years resulted in a suit of methods and techniques for solving them efficiently and reliably. A popular family of such methods is Variational Monte-Carlo, which parameterize a trial wave function and seeks to optimize the parameters in order to minimize the expected energy, thus approximating the ground state of the system. While classic VMC methods, such as trial wave functions with Jastrow factors, have proved useful, they come with some weaknesses: The inflexibility of the trial wave function may lead to poor approximations of the real ground state, even if a global minimum in energy for the particular trial wave function was obtain. Further, observables are hard to estimate from trial wave functions, because popular methods for sampling, such as MCMC, tends to produce data with high degree of auto-correlation(sitat). This is even more true for larger systems, and leads to a high statistical uncertainty in estimated observables.

In recent years, drawing inspiration from Deep Learning, Artificial Neural Networks have been employed as trial wave functions with great success (sitat). Because of the huge number of parameters, Artificial Neural Networks tend to be much more flexible than classical Trial Wave Functions. However, this results in a greater challenge to optimize the parameters, and the usual problem with auto-correlated samples is still present.

To address the latter problem, some papers have very recently succeeded in employing auto-regressive models on spin-systems, such as Quantum Ising-model. To obtain a spin-configuration, each spin is sampled in sequence, each time conditioning on the previous sampled spins. Because of the nature of auto-regressive models, all sampled spin-configurations are uncorrelated, removing the problem with high statistical variance in estimating observables.

In this paper, we present an autoregressive model for bosonic quantum dots based on Recurrent Neural Networks, inspired by the work of (sitat).

II. THEORY

A. The System

1. The Potentials

The Hamiltonian under investigation describes N bosons in a potential trap, and is on the form

$$H = \sum_{i=1}^N \left(\frac{-\hbar^2}{2m} \nabla_i^2 + V_{\text{ext}}(\mathbf{r}_i) \right) + \sum_{i < j}^N V_{\text{int}}(\mathbf{r}_i, \mathbf{r}_j)$$

where V_{ext} is the external potential of the trap while V_{int} is the internal potential between the particles. The external potential has an elliptical form, being anisotropic in the z -direction:

$$V_{\text{ext}}(\mathbf{r}) = \frac{1}{2}m(\omega[x^2 + y^2] + \omega_z z^2) \quad (\text{II.1})$$

The internal potential is a hard shell potential, being infinite for distances where two bosons overlap:

$$V_{\text{int}} = \begin{cases} \infty, & \text{for } |r_i - r_j| \leq 0 \\ 0, & \text{otherwise} \end{cases}$$

2. Non-interacting Case

For non-interacting bosons in a spherical with $\beta = 1$ and $a = 0$ the system reduces to spherical harmonic oscillators where analytical solutions are available. The trial wavefunction reduces to simply the product of one body elements

$$\Psi_T(\mathbf{r}) = \prod_i^N \exp[-\alpha(x_i^2 + y_i^2 + z_i^2)] = \prod_i^N \exp(-\alpha|r_i|^2)$$

while the Hamiltonian reduces to

$$H = \sum_i^N \frac{-\hbar^2}{2m} \nabla_i^2 + \frac{1}{2} m \omega^2 r_i^2$$

which in natural units is

$$H = \frac{1}{2} \sum_i^N -\frac{1}{m} \nabla_i^2 + m \omega^2 r_i^2$$

Applying the Hamiltonian gives the local energy as

$$E_L = \frac{\alpha d}{m} N + \left(\frac{1}{2} m \omega^2 - \frac{2\alpha^2}{m} \right) \sum_i^N r_i^2$$

where d is the dimension. As the factor $\sum r_i^2$ is always positive, its term should be minimized, which is accomplished by setting $\alpha = \frac{m\omega}{2}$, giving a minimal local energy of

$$E_L = \frac{\omega d N}{2} \quad (\text{II.2})$$

3. Interacting Case

The local energy for the full interacting case is much more complicated. The full computation is deferred to appendix ???. The expression evaluates to

$$\begin{aligned} E_L = & -\frac{1}{2m} \sum_i \left[4\alpha^2 \left(x_k^2 \hat{\mathbf{i}} + y_k^2 \hat{\mathbf{j}} + \beta^2 z_k^2 \hat{\mathbf{k}} \right) \right. \\ & - 2\alpha(d-1+\beta) \\ & - 4\alpha \left(x_k \hat{\mathbf{i}} + y_k \hat{\mathbf{j}} + \beta z_k \hat{\mathbf{k}} \right) \sum_{l \neq k} \frac{\mathbf{r}_k - \mathbf{r}_l}{r_{kl}} u'(r_{kl}) \\ & + \sum_{i \neq k} \sum_{j \neq k} \frac{(\mathbf{r}_k - \mathbf{r}_i)(\mathbf{r}_k - \mathbf{r}_j)}{r_{ki} r_{kj}} u'(r_{ki}) u'(r_{kj}) \\ & \left. + \sum_{l \neq k} \left(u''(r_{kl}) + \frac{2}{r_{kl}} u'(r_{kl}) \right) \right] \\ & + \sum_i V_{\text{ext}}(\mathbf{r}_i) + \sum_{i < j} V_{\text{int}}(\mathbf{r}_i, \mathbf{r}_j) \end{aligned}$$

B. Variational Monte Carlo

In order to find a good candidate wavefunction for a given potential, one can employ the *variational principle*. One starts by guessing a trial wavefunction $|\Psi_T\rangle$ and estimating the trial energy, which is guaranteed

to be equal to or higher than the true ground state energy E_0 :

$$E_0 \leq E = \frac{\langle \Psi_T | H | \Psi_T \rangle}{\langle \Psi_T | \Psi_T \rangle} \quad (\text{II.3})$$

If $|\Psi_T\rangle$ is an eigenfunction of the Hamiltonian, the variance σ^2 will be minimal

$$\sigma^2 = \frac{\langle \Psi_T | H^2 | \Psi_T \rangle}{\langle \Psi_T | \Psi_T \rangle} - \left(\frac{\langle \Psi_T | H | \Psi_T \rangle}{\langle \Psi_T | \Psi_T \rangle} \right)^2 = 0$$

The variational principle expands on this idea by letting $|\Psi_T\rangle$ be a functional class of a *variational parameter* α . By varying α one can find the optimal trial wavefunction within the functional class by minimizing σ^2 .

Only a small collection of potentials have analytical solution using the variational principle. For most potentials, one must numerically integrate (II.3) using Monte Carlo integration.

For a stochastic variable x with probability density function $p(x)$, the average $\langle x \rangle$ is defined as

$$\langle x \rangle = \int_{\mathbb{R}} x p(x) dx$$

By sampling the stochastic variable M times, the average can be approximated by

$$\langle x \rangle = \int_{\mathbb{R}} x p(x) dx \approx \frac{1}{M} \sum_{i=1}^M x_i p(x_i)$$

Applying this to an observable \mathcal{O} , we have

$$\begin{aligned} \langle \mathcal{O} \rangle &= \langle \Psi | \mathcal{O} | \Psi \rangle \\ &= \int d\mathbf{r} \Psi^* \mathcal{O} \Psi \\ &= \int d\mathbf{r} |\Psi|^2 \frac{1}{\Psi} \mathcal{O} \Psi \\ &= \frac{1}{M} \sum_{i=1}^M p(\mathbf{r}) \mathcal{O}_L \end{aligned}$$

where $|\Psi|^2$ is defined as the probability density function, and $\frac{1}{\Psi} \mathcal{O} \Psi$ the *local operator*.

The local trial energy can then be defined as

$$E_L = \frac{1}{\Psi_T} H \Psi_T$$

which can be computed using Monte Carlo integration as

$$\langle E_L \rangle \approx \frac{1}{M} \sum_{i=1}^M p(\mathbf{r}_i) E_L(\mathbf{r}_i)$$

The goal is therefore to minimize minimizing $\sigma^2 = \langle E_L^2 \rangle - \langle E_L \rangle^2$ over the variational parameter α .

C. DNN and RNN

D. Autoregressive Models

E. Metropolis-Hastings

The estimate of the local energy relies on samples from the trial wave function. To get a physical value, the configuration of the particles must be as physical and probable. As the configuration achieving this is unknown, the configuration space must be explored. This is done through Monte Carlo simulation, more specifically by using the Metropolis-Hastings algorithm.

At each MC step a single particle is chosen at random, and a change to its position is proposed by moving it a fixed step length Δ and computing the ratio between new and old probability densities

$$\omega = \frac{P(\mathbf{r}_r, \dots, \mathbf{r}_k^*, \dots, \mathbf{r}_n)}{P(\mathbf{r}_r, \dots, \mathbf{r}_k, \dots, \mathbf{r}_n)} = \frac{|\Psi_T(\mathbf{r}_r, \dots, \mathbf{r}_k^*, \dots, \mathbf{r}_n)|^2}{|\Psi_T(\mathbf{r}_r, \dots, \mathbf{r}_k, \dots, \mathbf{r}_n)|^2}$$

where \mathbf{r}^* denotes a modified position. If the ratio ω is greater than a uniformly distributed number $\theta \in [0, 1]$, the move is accepted. This ratio can often be reduced analytically to obviate the need for recomputing the entire probability density each step.

F. Onebody Density

A useful way to understand a many body system is to integrate over all dimensions except for one, yielding the *one body density* $\rho(\mathbf{r})$, defined as

$$\rho(\mathbf{r}) = \int d\mathbf{r}_2 \dots d\mathbf{r}_N |\Psi_T(\mathbf{r})|^2$$

It is a scaled probability density function giving the number of particles within the volume $\Delta\mathbf{r}$ as $\rho(\mathbf{r})\Delta\mathbf{r}$. By convention the integral over all $d\mathbf{r}$ yields the total number of particles in the system, N .

III. METHOD

A. Architecture

B. Metropolis Sampling

C. Automatic Differentiation in Tensorflow

Since we are studying Hamiltonians defined on continuous space, calculating the Laplacian of the trial wave function is necessary to account for the kinetic energy of the system. Since the RNN-DNN model is made using the popular neural network framework

Tensorflow(2), it feels natural to use its automatic differentiation functionality to calculate the Laplacian of the model with respect to the inputs (the positions). However, for more than one dimensional input, it turns out to be quite difficult, although a work-around proposed by (sitat) resolved the difficulty. The problem was as follows:

Starting with an input x of dimension $(batch_size, d)$, a forward pass through the model results in an output y of dimension $(batch_size, 1)$, since the wave function evaluates to a scalar value. When performing **grad_y** = **tf.gradients(y, x)**, we get

$$grad_y = \left(\frac{\partial y}{\partial x_1}, \dots, \frac{\partial y}{\partial x_d} \right),$$

which has dimension $(batch_size, d)$. The problem arises when calculating the second derivative **grad2_y** = **tf.gradients(grad_y, x)**

$$grad2_y = \left(\sum_{i=1}^d \frac{\partial^2 y}{\partial x_1 \partial x_i}, \dots, \sum_{i=1}^d \frac{\partial^2 y}{\partial x_i \partial x_i} \right).$$

Since **tf.gradients** is meant to be used for gradient descent, a summation of the derivatives of all outputs w.r.t the input x is performed, which should not be present in the Laplacian. The naïve solution is to slice the output after the first differentiation, such as **tf.gradients(grad_y[i], x[i])**. Sadly, slicing this way does not respect the computational graph constructed during forward pass, and **x[i]** is interpreted as a new variable not related to **grad_y[i]**. The fix is to use clever reshaping of the input variable \mathbf{x} before passing it to the model, in order to allow for the wanted slicing without destroying the computational graph. Details can be seen in (sitat) and in our source code.

D. Optimization

During the training procedure of the RNN-DNN model, we use the following expression for the loss value:

$$L = 2 \sum_{i=1}^{N_B} \ln(\psi_i)(E_i - E)$$

where N_B is the batch size, ψ_i and E_i is the wave function and local energy of sample i in the batch, and E is the average local energy over the whole batch. During gradient decent, the derivative of the loss value is differentiated w.r.t. the model parameters, and the gradient describes (ref) is recovered.

During vanilla gradient decent, the parameters are updated by performing a small step in the opposite direction of the computed gradient

$$\theta \rightarrow \theta - \mu \nabla_{\theta} \langle E \rangle,$$

where θ is the parameters of the model, μ is the learning rate, and $\nabla_{\theta} \langle E \rangle$ is the derivative of the loss value.

As a better alternative to vanilla gradient decent, we use Tensorflows ADAM optimizer with default values, as it is a popular choice in the machine learning community.

E. One-Body Density

To extract a one-body density from a Monte-Carlo simulation, we partition space into a number of bins in an appropriate range where the wave function is large. The bin size can be chosen small to get finer details of the density, but will require more data to mitigate statistical error.

For each particle configuration produced at every Metropolis step, the number of particles coinciding with each bin is checked. The one-body density is then produced by averaging over all Metropolis steps.

IV. RESULTS AND DISCUSSION

If not otherwise specified, the results have been derived using the following parameters:

- Harmonic oscillator frequency $\omega = 1$
- Coulomb interaction strength and shielding constants $\alpha = 1$, $\beta = 0$
- Metropolis step length $step_length = 1$
- Number of Metropolis steps $steps = 20$
- Batch size of 500
- Training duration of 500 epochs
- Two layer DNN architecture with 32 nodes each

A. Pure DNN Model for One Particle In Harmonic Oscillator

1. One Particle in 1D Harmonic Oscillator, Relu vs Tanh

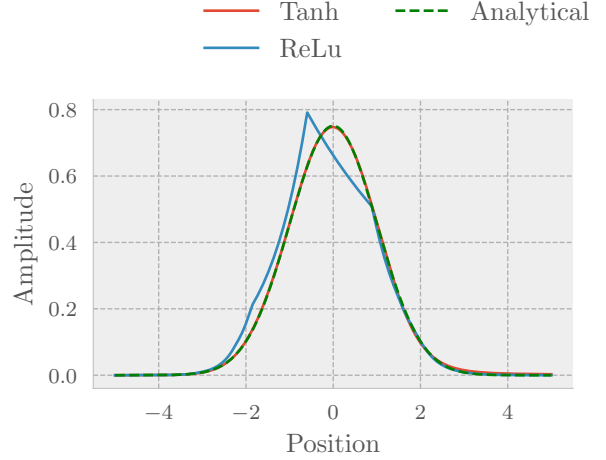


Figure IV.1: Wave function of particle in 1D harmonic oscillator, $\omega = 1$, approximated using DNN with Tanh and ReLu activations, respectively. The Metropolis step length was set to 2. The results are plotted against the analytical result

In figure Figure IV.1, we see the result of training the DNN trial wave function on a single particle in a 1D harmonic oscillator. The Metropolis step length was set to 2 to yield $\approx 50\%$ acceptance rate. Upon first exception, we see that the trial wave function using *ReLU* as activation fails spectacularly in approximating the analytical result, while *Tanh* produces a very close approximation.

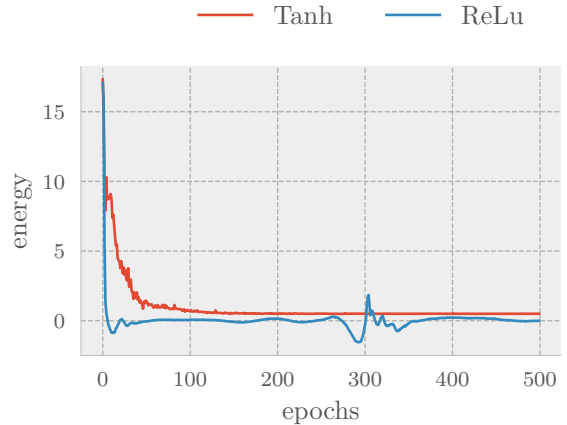


Figure IV.2: Energy estimated from each batch during training of the *Tanh* and *Relu* model on one particle in 1D harmonic oscillator

The minimization of $\langle E \rangle$ during training for the *ReLU* and *Tanh* model can be seen in Figure IV.2, and reveals even more serious problems with *ReLU*. While the energy of the *Tanh* model smoothly decreases towards the analytical value of $E = 0.5$, the energy of the *ReLU* model varies wildly, even undercutting the analytical value. This is disastrous, as it violates the variational principle.

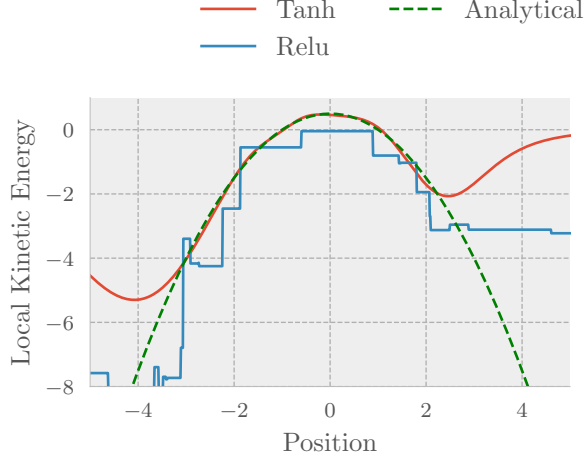


Figure IV.3: Local kinetic energy of the *Tanh* and *Relu* model trained on one particle in 1D harmonic oscillator

Figure IV.3 shows the local kinetic energy (the kinetic term entering the local energy) as a function of position for the *ReLU* and *Tanh* model. This is plotted against the analytical result. As can be seen, the local kinetic energy of *ReLU* model is very ill-behaved, is most likely the cause of the violation of the variational principle. Since the local kinetic energy relies on the Laplacian of the trial wave function, the use of activation functions with discontinuous derivatives, such as *ReLU*, appears to produce models which cannot approximate wave functions with appropriate curvature.

Further, Figure IV.3 shows an interesting feature of the *Tanh* model. While it closely approximates the correct local kinetic energy in the center part, it fails for positions far from origo. A possible explanation is that since we are producing samples using the Metropolis algorithm, configurations corresponding to where the wave function is small-valued will be sampled less often. As a result, the model may struggle to learn the correct approximation of the kinetic term for these areas. However, this may not be a problem for numerical accuracy, since the same configurations that the model struggle to learn will seldom be sampled, and will not contribute much to expectation values.

2. One Particle in 2D and 3D Harmonic Oscillator

Seeing the failure of *ReLU*, the switch to only *Tanh* is made.

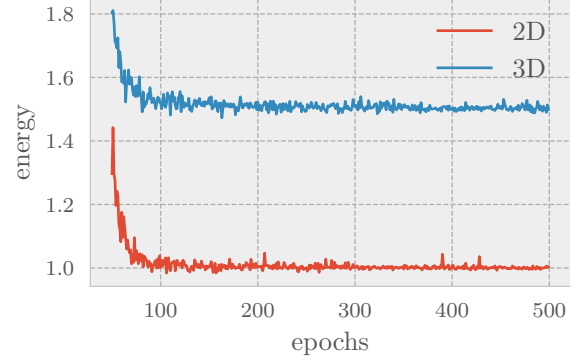


Figure IV.4: Energy estimated from each batch during training of the DNN model on one particle in harmonic oscillator, in 2D and 3D, respectively

The minimization of $\langle E \rangle$ during training of the DNN model on one particle in 2D and 3D harmonic oscillator can be seen in Figure IV.2. Both energies approach the correct ground state energy, respectively $E = 1$ and $E = 1.5$ in two and three dimensions. Note also that towards the end of training, the fluctuations in the estimated energies die down. This is an indication that the trial wave function approaches the correct ground state, as $\sigma^2 = 0$ when $\psi_{\text{Trial}} = \psi_{\text{GS}}$.

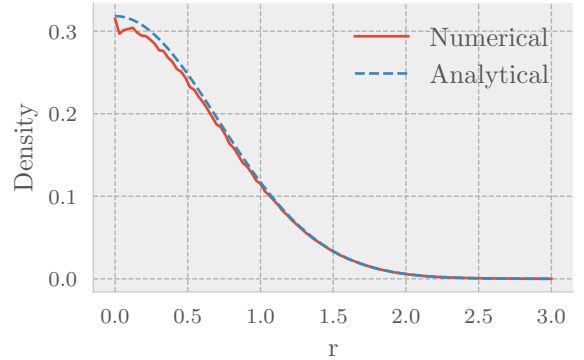


Figure IV.5: Radial one-body density for one particle in 2D harmonic oscillator. The density was calculated using $N = 1e6$ samples from the trained DNN model, using 100 bins on the interval $[0, 3]$. It is compared to the analytical result

B. RNN-DNN Hybrid Model for Non-Interacting Bosonic Quantum Dots

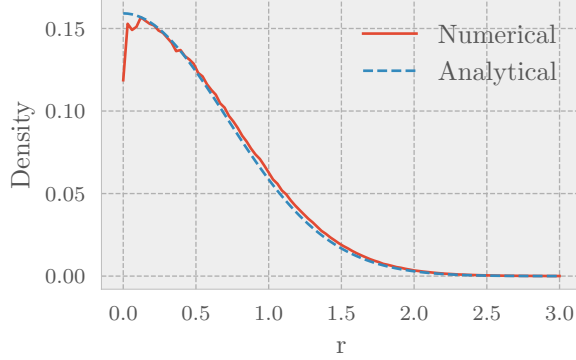


Figure IV.6: Radial one-body density for one particle in 3D harmonic oscillator. The density was calculated using $N = 1e6$ samples from the trained DNN model, using 100 bins on the interval $[0, 3]$. It is compared to the analytical result

After the previous training, the radial one-body density is calculated using $N = 1e6$ samples generated by the model. The densities are presented in Figure IV.5 and Figure IV.6. Although the approximation is not as close as seen in Figure IV.1, it is still fairly good.

3. Ground State Energies

	Numerical	Analytical
1D, Tanh	0.5015(2)	0.5
1D, ReLu	0.0032(2)	0.5
2D, Tanh	1.0015(1)	1
3D, Tanh	1.5046(1)	1.5

Table IV.1: Summary of the estimated ground state energies of the DNN model trained on the previously discussed systems. The energy was estimated using $N = 1e6$ samples

In Table IV.1, a summary of the estimated ground stated energies of the DNN model trained on the previously discussed systems is presented. Without too much concern for choice of parameters, such as batch size, number of metropolis steps, or network architecture, all models but the Relu model produces results to accurate to 1% – 3%.

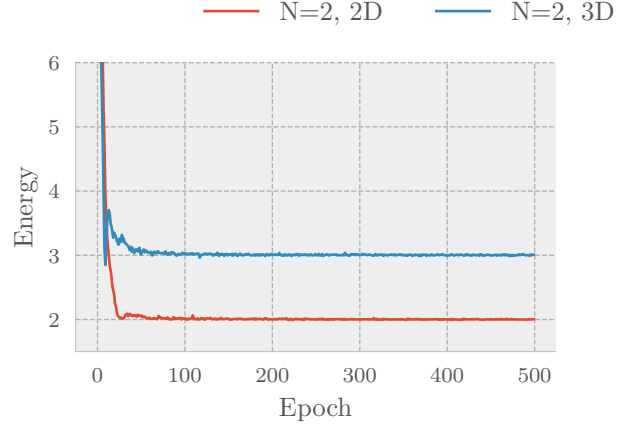


Figure IV.7: Estimate of energy during training of RNN-DNN hybrid models. The models were trained on two non-interacting bosons in 2D and 3D harmonic oscillator. The models were trained for 1000 epochs, using a batch size of 500.

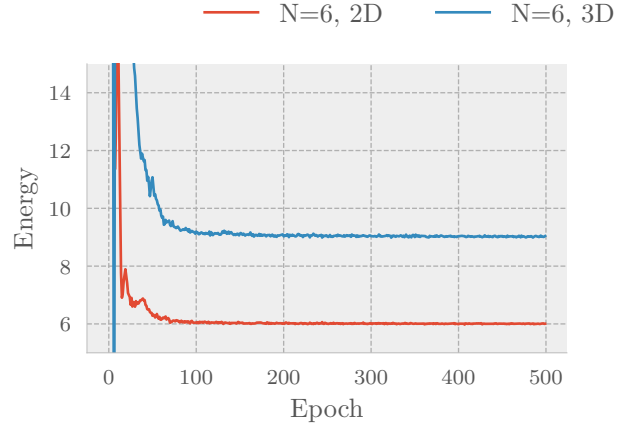


Figure IV.8: Estimate of energy during training of RNN-DNN hybrid models. The models were trained on six non-interacting bosons in 2D and 3D harmonic oscillator. The models were trained for 1000 epochs, using a batch size of 500.

In Figure IV.7 and Figure IV.8, we see the minimization of energy as the RNN-DNN model is trained on various numbers of non-interacting bosons in 2D and 3D harmonic oscillators. In all cases, the model used a hidden state of 5 units, together with a two layer network with 32 nodes each. Although the RNN-DNN uses the hidden state to encode the correlation with previously sampled particles, it has no problem learning the ground state of uncorrelated systems, as seen

in the figures. Note that in [Figure IV.8](#), a sudden dip in the energy in the beginning training can be seen for $N = 6$ in 3D. This dip violates the variational principle. As nothing was done to regularize the trial wave function, it is perhaps unnormalizable during early stages of training, since the initial parameters are random. This will likely cause the metropolis algorithm to fail, as it is not possible to sample from such a distribution. Nevertheless, the model approaches the correct ground state energy.

	Numerical	Analytical
N=2, 2D	2.0017(5)	2
N=6, 2D	6.0044(8)	6
N=2, 3D	3.0021(5)	3
N=6, 3D	9.012(1)	9

Table IV.2: Summary of the estimated ground state energies of the RNN-DNN model in the non-interacting case. The energy was estimated using $N = 1e5$ samples

From [Table IV.2](#), we see that the RNN-DNN model attains good accuracy for the non-interacting case, both in 2D and 3D, averaging a relative error of 0.1%.

C. RNN-DNN Model for Two Interacting Bosonic in 1D Quantum Dots

1. Training

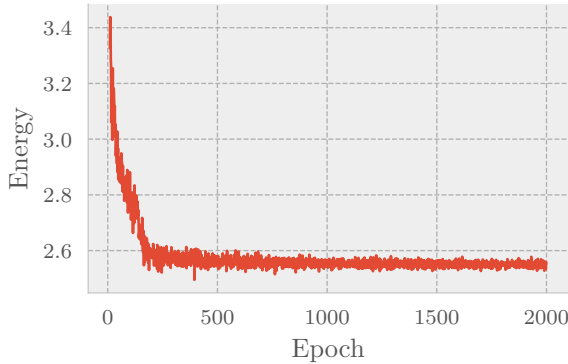


Figure IV.9: Estimate of energy during training of RNN-DNN hybrid model. The model was trained on two interacting bosons in 1D harmonic oscillator. For the Coloumb interaction, a strength value of $\alpha = 1$ and a shielding value of $\beta 0.1$ was used. The models were trained for 2000 epochs, using a batch size of 2000.

In [Figure IV.9](#), we see the training process of two interacting bosons in 1D harmonic oscillator. The minimization of the energy is a bit more noisy than the previous non-interacting cases, hence the batch size was increased. The model used a hidden state of

5 units, together with a two layer network with 64 and 32 nodes, respectively.

Using $N = 1e6$ samples, the ground state energy was estimated to be $E = 2.552(1)$. Compared to $E = 2.5482$ CISD energy using 40 orbitals(courtesy Øyvind Schøyen), the relative error is about 0.1%.

2. One-Body Density

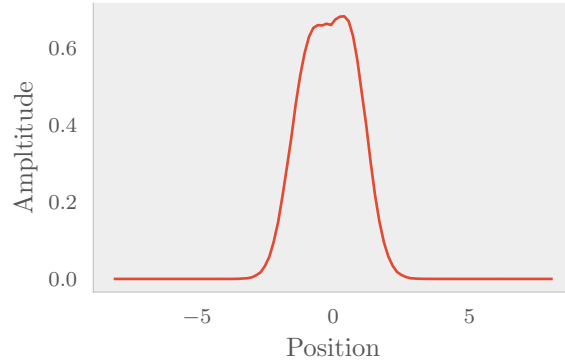


Figure IV.10: One-body density for two interacting bosons in 1D harmonic oscillator. The density was calculated using $N = 4e5$ samples and 100 bins on the interval $[-8, 8]$.

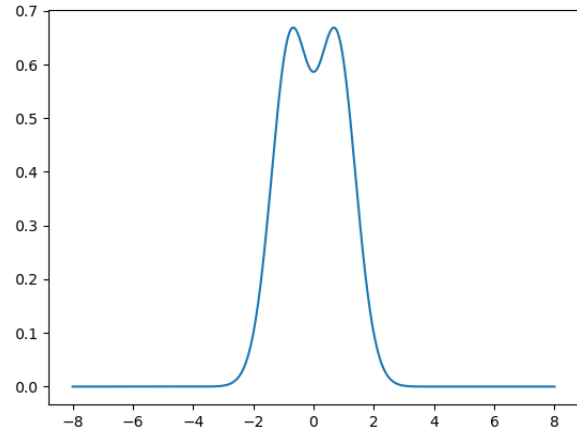


Figure IV.11: One-body density for two interacting bosons in 1D harmonic oscillator using CISD, courtesy Øyvind Schøyen

[Figure IV.11](#) shows the corresponding one body density, which shows the characteristic separation of two peaks caused by the repulsive interaction. Comparing with the one-body density produced with the CISD simulation, the peaks are not as sharply defined. In

terms of ground state energy, the RNN-DNN model successfully accounts for the correlation of the system, showing that the hidden state is able to encode the correlation in a meaningful way. However, like other approaches in machine learning VMC, such as RBM, it struggles to reproduce the correct one-body density.

3. Conditional Probabilities

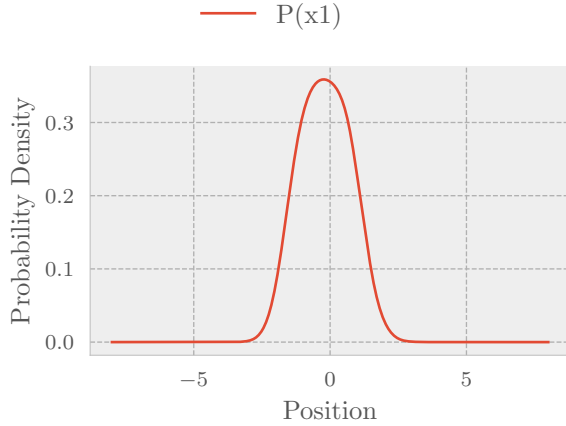


Figure IV.12: One-body density for two interacting bosons in 1D harmonic oscillator. The density was calculated using $N = 4e5$ samples and 100 bins on the interval $[-8, 8]$.

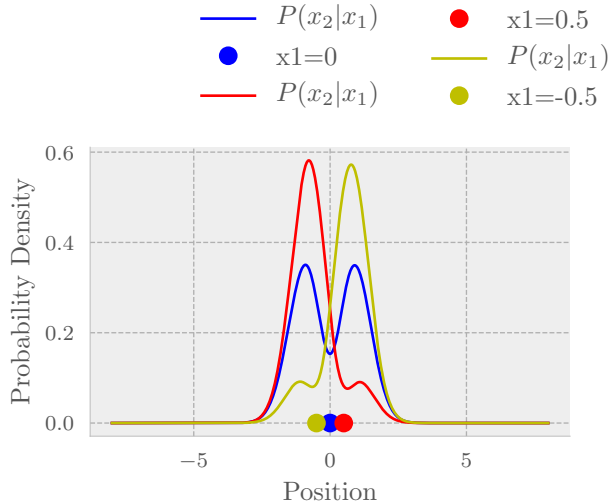


Figure IV.13: One-body density for two interacting bosons in 1D harmonic oscillator. The density was calculated using $N = 4e5$ samples and 100 bins on the interval $[-8, 8]$.

In Figure IV.12 and Figure IV.13, we see the conditional probabilities produced by the RNN-DNN model trained on two interacting bosons in 1D harmonic oscillator. In Figure IV.12, we see that the probability density for particle 1 is skewed towards the left. As there is no physical reason for why the first sampled particle is found more often to the left, one should think of the conditional probabilities more as rules for sampling the particles, rather than physical objects. In fact, given $P(x_1, x_2)$, there is no unique way of factoring it to conditional probabilities:

$$P(x_1, x_2) = P(x_1)P(x_2|x_1) = f(x_1)P(x_1) \frac{P(x_2|x_1)}{f(x_1)} = \tilde{P}(x_1)\tilde{P}(x_2|x_1),$$

where $f(x_1)$ is an arbitrary function.

In Figure IV.13, we see however that some physical meaning is retained. The probability density of particle two conditioned on particle one's position act as to avoid particle one. Given particle one's position, the probability of sampling particle two's position close to it is relatively small compared to sampling it further away. This is a reflection of the repulsive potential, which pushes the particles apart.

4. Sampling from Conditional Probabilities

Next, we inspect if using BruteForce Metropolis to sample from distributions produce densities that are faithful to that distribution.

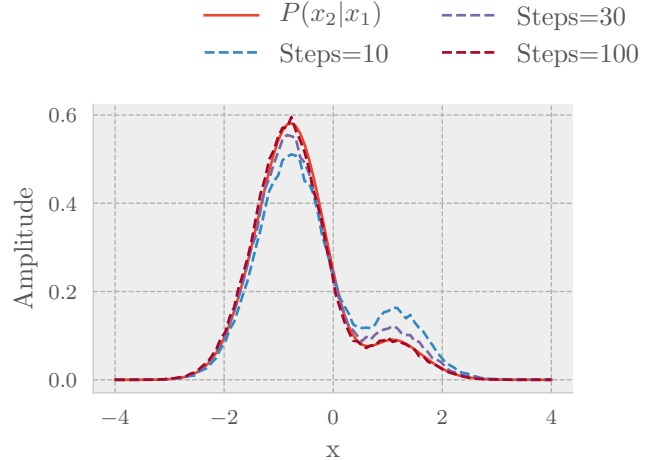


Figure IV.14: One-body density for two interacting bosons in 1D harmonic oscillator. The density was calculated using $N = 4e5$ samples and 100 bins on the interval $[-8, 8]$.

In Figure IV.14, the target probability density is $P(x_2|x_1 = 0.5)$ produced by the RNN-DNN model

trained on the system as previously discussed. The densities were estimated using Bruteforce Metropolis with a step length of 1 and a varying number of thermalization steps. For a low number of steps, such as 10, it can be seen from the figure that the estimated density does not match the one produced by the model. Since the random walkers start off uniformly, they need a sufficient amount of steps so that they don't end up getting stuck in low probability areas, as seen to the left in the figure. If this happens, we fail to sample variables that are distributed as our model dictates. From the figure, we see that a increased number of steps remedy this.

2. One-Body Density

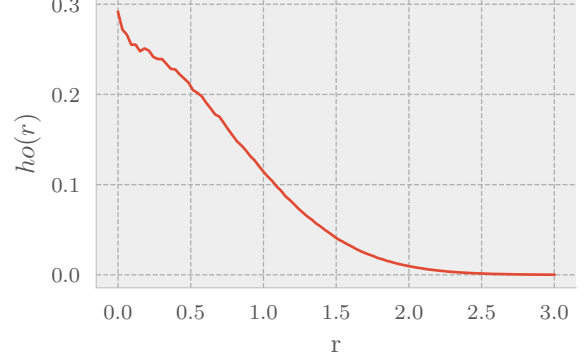


Figure IV.15: One-body density for two interacting bosons in 1D harmonic oscillator. The density was calculated using $N = 4e5$ samples and 100 bins on the interval $[-8, 8]$.

D. RNN-DNN Model for Two Interacting Bosonic In Higher Dimension

1. Ground State Energy

	RNN-DNN	DMC
2D	3.014(3)	3.00000(1)
3D	3.751(1)	3.730123(3)

Table IV.3: Estimated ground state energies of the RNN-DNN model train on two interacting bosons in 2D and 3D harmonic oscillator, respectively. In both cases, 10 hidden units and two layers of 64 and 32 nodes were used. The batch size was 4000 and the models were trained for 1000 epochs. The energy was estimated using $N = 1e5$ samples.

From Table IV.3, we see the estimated ground state energy of the RNN-DNN model trained on two interacting bosons in 2D and 3D harmonic oscillator. Taking the DMC calculation as ground truth, the numerical error is under 1% in 2D and 3D, as with the 1D case.

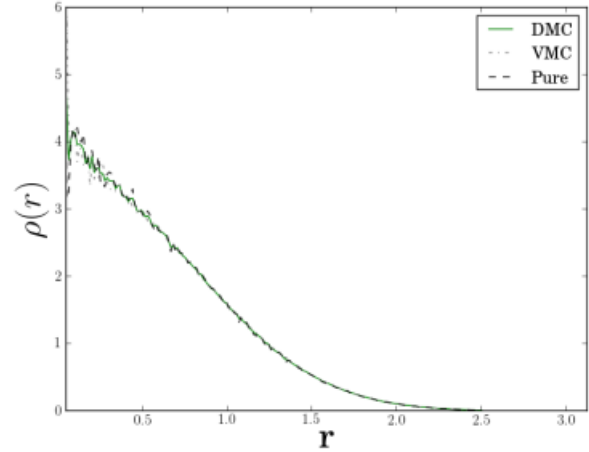


Figure IV.16: One-body density for two interacting bosons in 1D harmonic oscillator. The density was calculated using $N = 4e5$ samples and 100 bins on the interval $[-8, 8]$.

In Figure IV.15 and Figure IV.16 we see the radial one-body density of two interacting bosons in 3D harmonic oscillator calculated using our RNN-DNN model and DMC, respectively. Note that technically, the DMC calculation was performed on a two electron system, but since this state is symmetrical with respect to spatial coordinates, it is comparable to our bosonic system. In addition, the density is not scaled.

Since the figures are produced independently, they are hard to compare. However, some general features can be seen: 1/3 of the max amplitude occur around $r = 1$, and the density have almost completely diminished around $r = 2$. On the other hand, the density produced

by the RNN-DNN model is not as linear towards the origin as the DMC density, again indicating the our model may struggle reproducing the correct one-body density.

V. CONCLUSION

VI. FUTURE WORK

Appendix A